ELSEVIER

Chemical Physics 258 (2000) 121–137

Chemical Physics

www.elsevier.nl/locate/chemphys

The radial distribution functions of water and ice from 220 to 673 K and at pressures up to 400 MPa

A.K. Soper *

ISIS Department, Rutherford Appleton Laboratory, Chilton, Didcot, Oxon OX11 0QX, UK

Received 13 June 2000

Abstract

Neutron diffraction data for water and ice in the form of OO, OH and HH partial structure factors now exist over a temperature range 220–673 K, and at pressures up to ~400 MPa. In order for these data to be useful for comparing with different computer simulations and theories of water, it is first necessary to Fourier transform them to the corresponding site–site radial distribution functions. The process of doing this is not straightforward because of the inherent systematic uncertainties in the data, which arise primarily in the case of neutron scattering, from the inelasticity or recoil effects that can distort the experimental data. In this paper, it is shown that the empirical potential structure refinement procedure, which attempts to fit a three-dimensional ensemble of water molecules to all three partial structure factors simultaneously, leads to improved reliability in the extracted radial distribution functions. There are still some uncertainties, primarily associated with the hardness of the repulsive core of the intermolecular potential, which current data are not precise enough to resolve. The derived empirical potentials show some variability associated with particular experiments. General trends can be discerned however which indicate polarisation effects may be significant when effective intermolecular potentials are used over a wide temperature and density range.

1. Introduction

It is generally recognised that obtaining a reliable set of radial distribution functions for water has to be an essential prerequisite in any attempt to understand the properties of water and aqueous systems at the atomic level. The reasons for this are several. Firstly, reliable radial distribution functions are one of the crucial yardsticks against which any computer simulation or theory of water must be tested. Very few published computer simulations of water exist which do not at some point make a comparison with some form of diffraction experiment. Secondly, when attempting to understand the effect of dissolved substances on water it is essential to be able to compare the structure of the modified solvent in the presence of the solute with that of the pure solvent. This comparison is an important indication of how the solute–solute interaction may be modified when dissolved in water. Thirdly, the thermodynamic state dependence of the structure of water is, at least in principle, an indispensable guide to the non-pairwise-additive terms in the interatomic potential. Finally, the pronounced hydrogen bonding between water molecules, combined with the particular molecular geometry of the water molecule, gives rise to quite distinct forms for the

* Tel.: +44-1235-445543; fax: +44-1235-445642.
E-mail address: a.k.soper@rl.ac.uk (A.K. Soper).

0301-0104/00/$ - see front matter
PII: S0301-0104(00)00179-8

OO, OH and HH radial distribution functions [1], in a way which is not reproduced by other molecular systems. See for example, equivalent diffraction work on the hydrogen halides [2–4], hydrogen sulphide [5], and ammonia [6]. The structure of water is therefore fundamentally important for characterising the nature of the hydrogen bond at the atomic level.

Since the early 1980s, it has been shown that it is possible to extract the partial structure factors for water using the technique of hydrogen/deuterium substitution in combination with neutron diffraction [7,8]. This is because the hydrogen atom has a marked difference in neutron scattering length compared to deuterium, and because the neutron is scattered directly from the nucleus. Thus, by making diffraction measurements on heavy water, light water and at least one mixture of these two liquids, the corresponding nucleus–nucleus partial structure factors can be extracted by inverting the scattering matrix corresponding to each diffraction dataset [1]. The fundamental assumption behind the neutron experiment is that the structures of heavy water and light water are isotope independent, whereas earlier quantum computer simulations [9] and now X-ray data [10] indicate that the two liquids may well be slightly different in structure. If this is the case, then it should be noted that this does not automatically rule out the possibility of doing isotope substitution on water. There is so far no indication that the two liquids are different in structure by more than a few percent in the radial distribution functions, and it was shown previously that an isotope substitution experiment in that case would measure the average structure of the two liquids [1]. In practice, the uncertainties in the neutron experiment are typically likely to be significantly greater than the difference in structure due to quantum effects, so the differences between the two liquids are usually ignored. However, the possibility of these differences being present, and in particular becoming more apparent at low temperature must always be borne in mind when considering neutron diffraction experiments on water.

The neutron data can in principle be supplemented by X-ray diffraction data, which, particularly with modern synchrotron sources, can be extracted with significantly better statistical precision than the neutron data. Analysis of the X-ray data is also non-trivial, however, since it requires knowledge of the electron form factor of the molecule, which due to the highly polarised nature of the water molecule in the liquid, is not known to any accuracy. In addition, the X-ray experiment is primarily sensitive to the O–O structure factor and so can give little direct information on the hydrogen bonding in water. This information can be obtained only by inference in the X-ray experiment, by analysing the behaviour of the second peak in the OO radial distribution function with changes in pressure and temperature [11].

By far, the greatest controversy in experimental determinations of water structure arises from the process of converting the measured diffraction data to site–site radial distribution functions. The conventional practice of performing a simple Fourier transform on the data is prone to introducing serious truncation and systematic errors into the resulting radial distribution functions, and this has led to statements about water structure above the critical point [12] being made which were subsequently shown to be controversial [13,14]. Pusztai has recently attempted to extract the radial distribution functions from diffraction data by fitting the total scattering patterns instead of the partial structure factors [15] using a reverse Monte Carlo (RMC) procedure. His results so far diverge significantly from other attempts using Fourier transform methods on both the extracted partial structure factors [1,7], and on the total scattering patterns [16–18]. They also disagree with other recent attempts using Monte Carlo simulation procedures [19,20].

There are two primary sources of error in the diffraction data on water. Firstly, especially with neutrons, and also with X-rays if energy analysis is used to remove the Compton scattering, the data can only be obtained with finite statistical uncertainty. In general, the statistical uncertainty is worse at large values of the wave vector transfer, Q, which has the effect of making it difficult to determine at precisely which value of Q the structural oscillations disappear. In addition for the OH and HH structure factors, the diffraction pattern has oscillations due to the intramolecular

interferences which proceed to large Q. Measuring these oscillations precisely is an essential prerequisite to determine the *intra*molecular structure. Thus, finite counting statistics give rise to an effective truncation of the diffraction data, resulting in a loss of resolution in real space.

The second main source of error comes from the need to estimate the single atom scattering for neutrons or the single electron (Compton) scattering for X-rays. This scattering does not contain useful information on the relative arrangement of atoms or electrons, but it does constitute a significant part of the diffraction pattern. It is the single atom or single electron scattering about which the useful interference signal oscillates. Therefore, any error in estimating this single particle scattering can give rise to potentially significant errors in estimating the interference signal. In both X-rays and neutron scattering, the single atom or electron scattering is subject to substantial recoil distortion by the scattering radiation and attempts to estimate this effect invariably prove to be approximate at best. The main features of the recoil or Compton distortion however is that it is *additive* to the total scattering pattern, and that it is unlikely to have the kind of oscillatory structure seen in the interference signal. Therefore, it has to be regarded as a form of (generally unknown) background on top of which the true oscillatory structure is added.

A third aspect, relevant particularly to the neutron experiment, is that the nuclear recoil distortion is neutron *energy* dependent, rather than Q dependent. If the neutron measurements are made using an energy dispersive technique as at a pulsed neutron source such as ISIS, the same Q values are scanned over a range of different neutron incident energies using neutron detectors at different scattering angles. This means that the recoil distortions, which are substantial for neutrons scattered by light hydrogen, will to some extent be blurred when the different detector arrays are combined at a given Q value, whereas the genuine interference signal will be amplified in the combination.

For all these reasons therefore, there is considerable scope to develop a practical process for extracting the radial distribution functions from experimental diffraction data on water. It will be essential that the nature and source of the errors be understood and taken into account. A premise of this paper and much of the work that has preceded it is that there *are* errors in the data. If however we are careful enough in the way we set up our structure refinement process, we should be able to prevent much of that error being carried through to the calculated radial distribution functions.

The rest of this paper therefore is devoted to the application of a particular computer simulation technique, called empirical potential structure refinement (EPSR), to the process of estimating the radial distribution functions of water. The method has been applied to all the available neutron data on water and ice, from 220 to 673 K, some of which have not hitherto been published, and the results of this analysis are given here. The diffraction data used here have been derived entirely from neutron diffraction experiments, and unless otherwise noted, were obtained on the small angle neutron diffractometer for amorphous and liquid samples (SANDALS) at ISIS.

2. Empirical potential structure refinement

The object of this procedure is to set up a model ensemble of water molecules whose partial structure factors agree as close as possible with those obtained from diffraction data [20]. This process is closely analogous to what has been done with crystallographic data for many years. Since the system is disordered, the only practical way to model the structure is via a computer simulation. In the case of water, the primary constraints on the distribution of water molecules is that they must have the correct density, the correct intramolecular geometry, and of course the modelled distribution must reproduce the diffraction measurements as close as practical. EPSR is a technique for achieving that goal.

2.1. Setting up the interaction potential

The potential in the EPSR method [20] consists of three principal terms. An *intramolecular* harmonic potential is used to define and maintain the molecular geometry. A *reference* intermolecular potential provides the starting point for the

simulation to get the molecules into a realistic region of configurational space. A perturbation, called the *empirical* potential, is then added to the reference potential to drive the simulation as close as possible to the experimental data.

A large number of computer simulations of water are of course available in the literature and will not be referenced here in any detail. The majority of water simulations are performed with water molecules in which the atoms are precisely localised with respect to the molecular axes, but even when the molecules are not rigid, the simulations almost invariably treat the intramolecular motion using classical mechanics. This immediately runs into a problem when attempting to compare with diffraction data, since the intramolecular structure of molecules in the real liquid is dominated by quantum mechanical zero-point disorder which has no classical analogue, and certainly must be included in any simulation which is to be compared directly with the diffraction data.

The starting point of the EPSR simulation therefore is to build an ensemble of molecules whose internal structure reproduces that which can be obtained from the diffraction experiment. Essentially, each intramolecular distance is characterised by an average distance, $d_{\alpha\beta}$, and a width, $w_{\alpha\beta}$, and the intramolecular structure is established by assuming the atoms in each molecule interact via a harmonic potential. The total (dimensionless) intramolecular energy of the system is represented by

$$U_{\text{intra}} = C\sum_i \sum_{\alpha\beta\neq\alpha} \frac{(r_{\alpha_i\beta_i} - d_{\alpha\beta})^2}{w_{\alpha\beta}^2}, \tag{1}$$

where $r_{\alpha_i\beta_i}$ is the actual separation of the atoms α, β in molecule i, $w_{\alpha\beta}^2 = 1/\sqrt{M_\alpha M_\beta}$, M_α is the mass of atom α in atomic mass units, and C is a constant determined from the diffraction data. All the simulations reported here used $C = 40$ Å^{-2}, determined by comparing the simulated structure factors with the measurements at large Q. The same value of C was used for all temperatures, since the zero-point disorder was not anticipated to be strongly temperature dependent, and there was little evidence for a temperature dependence in the data. The intramolecular distances used were $d_{\text{OH}} = 0.976$ Å and $d_{\text{HH}} = 1.550$ Å, which values were determined to give the best fit to the data. Again no significant temperature dependence on these intramolecular distances was found. It must be emphasised that the inclusion of non-localised atoms within the molecule does not constitute a degree of polarisability into the model: as described below intramolecular atom moves are made without reference to the intermolecular potential energy function. The intramolecular potential is used here only as a device to mimic the measured average molecular geometry. It does not contribute to the overall system Hamiltonian. When sampled with an exponential function (see Section 2.2) it reproduces the correct temperature-independent Gaussian disorder expected of zero-point motion.

The intermolecular reference potential is typically based on an intermolecular potential for water drawn from the literature. In principle, this potential can be as complicated as desired, but most of the simulations reported here used the same Lennard-Jones and charge parameters as the simple point charge extended (SPC/E) potential [21]. A few of the present simulations have used a modified version of this, as described below. This potential was derived for rigid molecules and so will not necessarily be appropriate to the kind of disordered molecules used in EPSR simulations. Nonetheless it gave a reasonable description of the local order in water (Figs. 1–3) and so was a useful point from which to start the structure refinement.

The intermolecular reference potential energy is given by an expression of the form

$$U_{\text{inter}} = \frac{1}{2}\sum_{i,j\neq i}\sum_{\alpha,\beta}\left\{4\varepsilon_{\alpha\beta}\left[\left(\frac{\sigma_{\alpha\beta}}{r_{\alpha_i\beta_j}}\right)^n - \left(\frac{\sigma_{\alpha\beta}}{r_{\alpha_i\beta_j}}\right)^6\right] + \frac{q_\alpha q_\beta}{4\pi\varepsilon_0 r_{\alpha_i\beta_j}}\right\}, \tag{2}$$

where the sum is taken over all pairs of atoms on *distinct* molecules. For both the reference potentials used here $\varepsilon_{\text{OO}} = 0.65$ kJ mol^{-1}, $\varepsilon_{\text{OH}} = 0$, $\varepsilon_{\text{HH}} = 0$, $\sigma_{\text{OH}} = 0$, and $\sigma_{\text{HH}} = 0$, while for the SPC/E potential parameters $n = 12$, $\sigma_{\text{OO}} = 3.166$ Å,

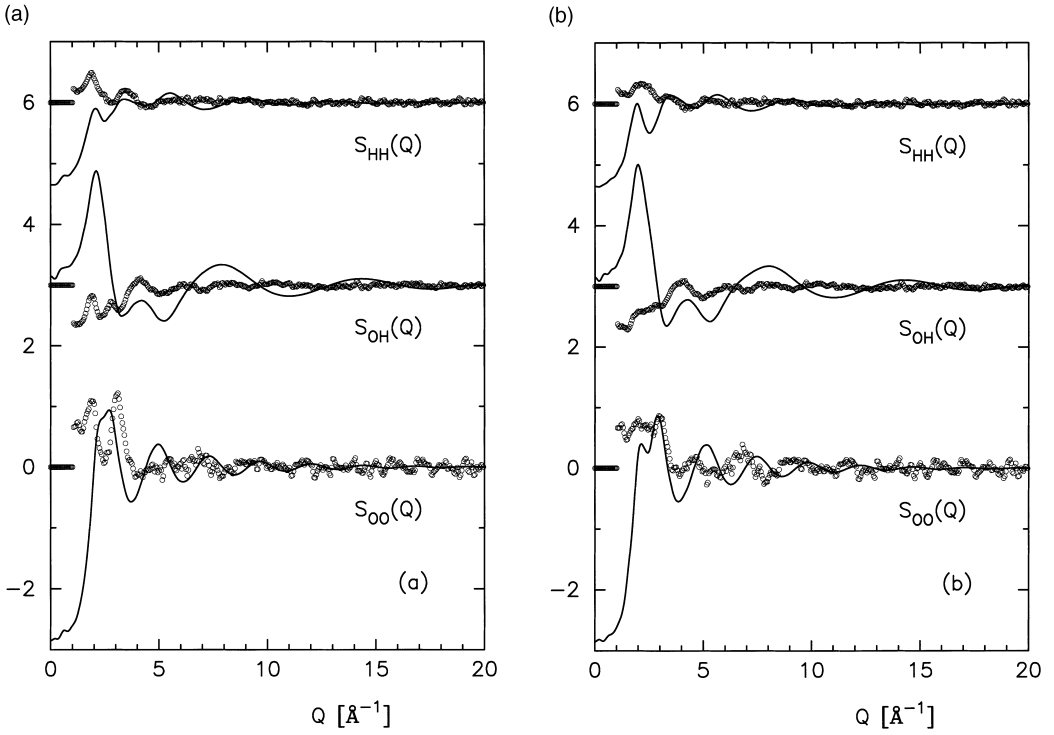

Fig. 1. Computer simulation of the OO, OH and HH partial structure factors of water at 298 K and 1 bar, using the SPC/E (a) and SPC10 (b) parameterisation of the reference potential as described in the text. The lines show the simulated structure factors, while the circles show the residual difference between neutron diffraction data and the simulated structure factors. Significant oscillations can be seen in these residuals, although the SPC10 simulation appears to give smaller residual oscillations than the SPC/E parameterisation. Note that all the structure factors in this paper are shown as per atom. Thus, they are three times greater in amplitude than if they were shown per molecule.

$q_O = -0.8476e$, and $q_H = +0.4238e$. For a few of the simulations (labelled SPC10), the parameters of the reference potential were set to $n = 10$, $\sigma_{OO} = 3.42$ Å, $q_O = -1.0e$, and $q_H = +0.5e$.

The perturbation to the reference potential, U_{epi}, is determined for each partial structure factor by taking the difference between experimental structure factor and simulated structure factor. The difference is Fourier transformed to r-space, using the minimum noise method [22] to ensure a minimum of truncation effects are transferred to the perturbation in r-space. Provided the perturbation at each iteration is not too large, this difference in r-space is equivalent to the difference between the potential of mean force for the experiment and that for the simulation. Having first equilibrated the simulation with the reference potential alone, the simulation is then run again using the reference potential plus perturbation potential until a new equilibrium is reached. The process is repeated iteratively, accumulating the perturbations to form the empirical potential, until such time as no further improvement in the fit to the data can be achieved. Because the refinement is simultaneously fitting all the available data at the same time, it is less likely to introduce effects in the radial distribution functions related to truncation, counting statistics and systematic errors in the data.

All intermolecular potentials, both reference and empirical, were truncated at half the box dimension with a function of the form $T(r) = 1/[1 + \exp\{20(r/r_c - 1)\}]$, with $r_c = 0.35D$, where D is the box dimension and r is the interatomic separation. This truncation function ensures that the intermolecular potential is essentially zero

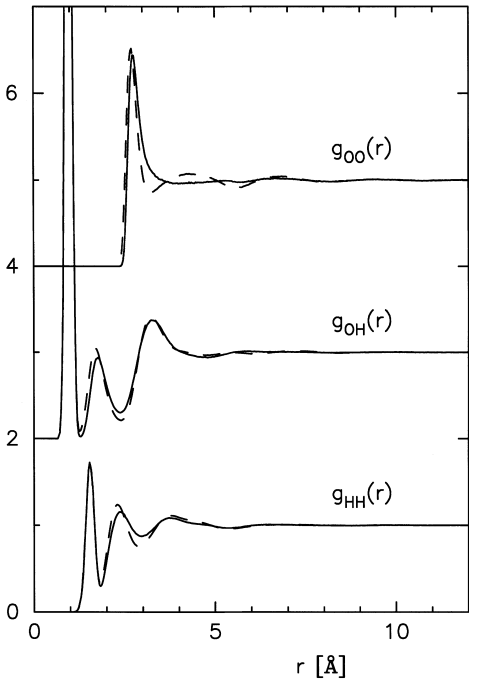

Fig. 2. Site–site radial distribution functions for the simulations shown in Fig. 1. Note that the second peak in the OO $g(r)$ is not well reproduced by the SPC/E simulation.

beyond half the box dimension. No correction was made for longer range forces in order that the simulation would proceed as quickly as possible, and because there was little information in the diffraction data on interactions greater than this distance. It is also generally believed [23] that long range corrections have little effect on the radial distribution functions of water.

2.2. Running the simulation

All the simulations were performed with 550 water molecules in a cubic box. The densities, temperatures and box sizes used in the simulations are given in Table 1. The standard minimum image convention was applied to calculate energies and radial distribution functions. Atomic and molecular moves are accepted or rejected on the basis of the conventional Metropolis Monte Carlo method [24].

There are three different kinds of moves within the EPSR simulation, namely individual atom moves where atoms are moved relative to one another within the molecule, molecular rotations and molecular translations, the latter two kinds of move being whole molecule moves. For more complicated molecules other moves can be envisaged, such as rotations of particular headgroups, or moves which keep the intramolecular distances the same but which change the symmetry of the molecule (e.g. left-handed to right-handed, etc.), but these are not relevant to the water simulations described here.

For the intramolecular moves, only the change in the intramolecular potential energy, ΔU_{intra}, is used to accept or reject the move. Thus, the probability of acceptance of an intramolecular move within the Monte Carlo scheme is based on the value of $\exp[-\Delta U_{\text{intra}}]$, i.e. there is no thermal factor in this sampling, in order to simulate zero-point disorder which is temperature independent to first approximation. If the data warranted a temperature dependence to this function (for example, in the event that intramolecular vibrational frequencies are altered radically by the changes in temperature and pressure) then this could be included in the value of C in Eq. (1). In fact, no significant temperature dependence has been observed in the present diffraction data.

For whole molecule moves, the usual Boltzmann thermal factor is used outside the intermolecular potential energies. In principle, whole molecule moves should not involve the relative movement of atoms within the molecule. However, computing round-off errors can accumulate over a number of such moves, so the intramolecular potential is included when calculating the total energy change. Thus, the probability of acceptance of a whole molecule move is based on the value of $\exp\left[-\left\{\Delta U_{\text{intra}} + 1/k_{\text{B}}T\left(\Delta U_{\text{ref}} + \Delta U_{\text{emp}}\right)\right\}\right]$, where for whole molecule moves ΔU_{intra} is normally expected to make only a small contribution to the total energy difference before and after the move. Since the intramolecular moves involve disordering individual molecules without reference to the surrounding molecules there are typically 50 whole molecule moves for each intramolecular move. In this way, the zero-point disorder of the molecules is simulated, while maintaining a realistic local molecular order.

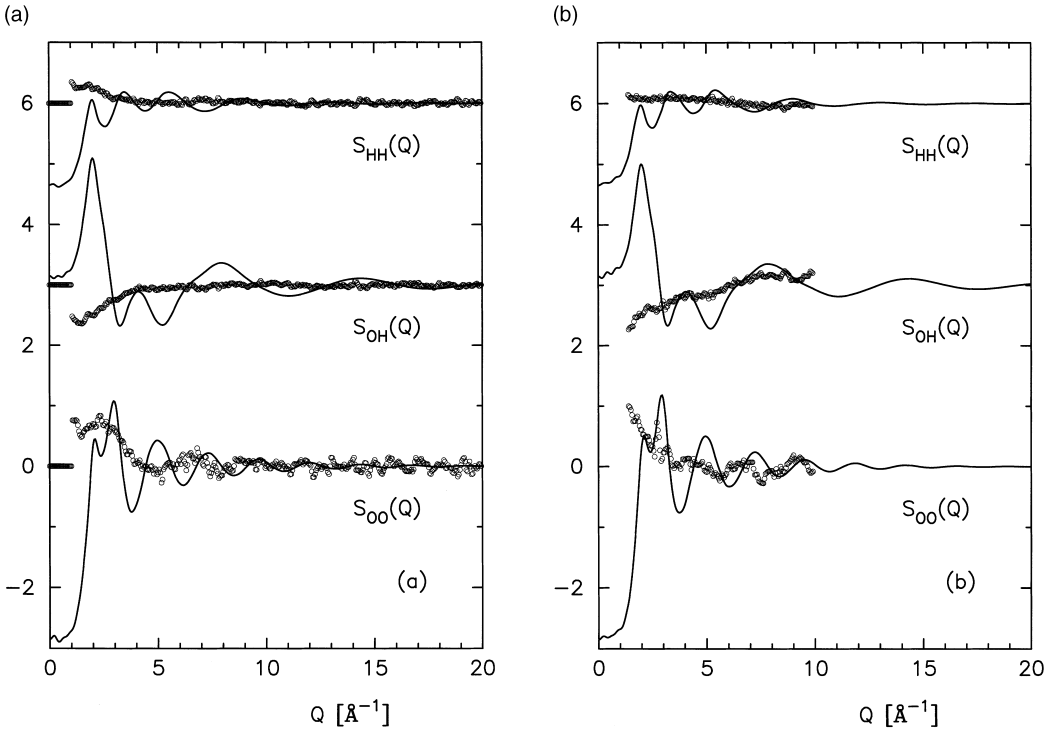

Fig. 3. EPSR of the OO, OH and HH partial structure factors for water at 298 K, 1 bar, using the SPC/E reference potential. The graph on the left corresponds to pulsed neutron time-of-flight diffraction data (a) [18], whereas that on the right corresponds the earlier reactor neutron diffraction data (b) [1].

One feature of EPSR simulation which is different from conventional simulation procedures is that the configurational energy and pressure of the simulation can be arbitrary. This is because the intermolecular potential energy function is being modified in a piecewise fashion without reference to the expected energy and pressure. With perfect data extending over a wide Q range, one might hope that the EPSR procedure would arrive at energies and pressures which were close to their measured values. With the imperfect data that are actually available this is never the case, although the intermolecular configurational energy values obtained in the present instance, as reported in Table 1, are at least of the correct sign and of the correct order of magnitude. Equally, the pressures obtained in the EPSR simulations (not shown here) were typically within ±200 MPa of the expected pressure.

In fact, a lower limit of –100 kJ mol^{-1} was placed on the configurational energy to prevent the empirical potential becoming excessively large or negative. In practice, this limit was only breached in the simulation of the ice data. In the event that the limit of –100 kJ mol^{-1} was exceeded the empirical potential was reduced in amplitude, without changing its shape, by a proportionate factor, in order to raise the energy of the simulation above this threshold.

The partial structure factors and site–site radial distribution functions derived from running the simulation with the intramolecular and reference intermolecular potentials alone (i.e. no empirical potential refinement) at $T = 298$ K are shown in Figs. 1–3, comparing them with the corresponding datasets. It can be seen that they give a sensible representation of the short range structure though some details in the partial structure factors are clearly incorrect. Given that the data may contain, as discussed above, some form of slowly varying, *additive*, systematic error, it is important to inspect the residual, that is the difference between data and

Table 1
Thermodynamic state points of the neutron diffraction runs on water in which OO, OH and HH partial structure factors were extracted by hydrogen isotope substitution[a]

Run label	Temperature (K)	Molecular number density (molecules per Å^3)	Experimental pressure (MPa)	Box size for simulation (Å)	Configurational energy (kJ mol^{-1})
268a	268	0.0338	27	25.3455	−78.6
268b	268	0.0362	210	24.7585	−79.9
268c	268	0.0381	400	24.3574	−88.3
298a	298	0.0334	(0.1)	25.4413	−28.9, −51.0
298b	298	0.0357	210	24.8750	−40.0
423a	423	0.0308	10	26.1379	−50.7
423b	423	0.0334	190	25.4413	−57.4
573a	573	0.0240	10	28.4043	−34.4
573b	573	0.0240	10	28.4043	−38.6
573c	573	0.0260	50	27.6565	−38.2
573d	573	0.0278	110	27.0462	−41.1
573e	573	0.0296	197	26.4864	−51.9
573f	573	0.0308	280	26.1379	−43.2
673a	673	0.0194	50	30.4764	−19.0
673b	673	0.0221	80	29.1960	−33.2
673c	673	0.0245	130	28.2174	−22.8
673d	673	0.0292	340	26.6220	−14.9
220a	220	0.0307	(0.1)	26.1662	(−100)

[a] Note that runs 573a and 573b were measured at the same thermodynamic state point, but at different times. The fifth and sixth columns list the box size and configurational energy obtained in the EPSR simulation. All simulations used 550 water molecules. The configurational energies are shown using the SPC/E parameterisation of the reference potential, with the exception of run 298a, which was run with both SPC/E and SPC10 reference potentials, and run 220a (ice) which was run only with the SPC10 potential. For 298a, the two values of the configurational energy correspond to the SPC/E refinement (left value) and SPC10 refinement (right value).

simulation, in order to detect the true level of fit. Simply quoting a standard deviation between simulation and data can be misleading in this situation. If this residual contains obvious oscillatory structure, it is likely the fit needs to be improved. If on the other hand the residual is non-zero, but slowly varying with wave vector, Q, it is likely that no further improvement in the fit can be achieved, since the residual then corresponds mostly to structure at unphysically short distances in the radial distribution functions. This is the signature that enables a genuine structural error in the simulation to be distinguished from a misfit caused by systematic error in the data. Hence, it is the residuals rather than the diffraction data which are shown in Figs. 1 and 2. As can be seen here, using the reference potential alone, with either the SPC/E or SPC10 parameters, does indeed leave visible oscillations in the residual, implying that the fit can be improved further.

3. Neutron diffraction experiments

Most of the diffraction data used here have been described elsewhere [1,18,25,26] and the references list, the relevant data analysis methods. With one exception, all the data were obtained on the SANDALS time-flight-diffractometer at ISIS, using the technique of hydrogen/deuterium isotope substitution to determine separate HH, OH and OO partial structure factors. This diffractometer, with its large solid angle of detectors concentrated at low scattering angles, is designed specifically for neutron diffraction from light atoms, such as hydrogen and deuterium. The one exception to this rule was that one set of data were obtained at the McMaster Nuclear Reactor much earlier than the others. These had been subject to a previous analysis [1] and so it was felt important to see how the present EPSR method of extracting radial distribution functions compares with previous

methods. In addition, the systematic errors in a reactor experiment are quite different to those in a time-of-flight experiment [7] and so this comparison will help to establish the likely accuracy of the results.

Two of the datasets, the one at 298 K and 210 MPa, and the data on ice at 220 K, have not been published before, though the former were referred to in a previous publication [25]. The sample container used for pressurised water is the same as that described previously for superheated water [27].

Ice presents a significant challenge for the analysis in the manner prescribed here, since it is important to have diffraction data on an absolute scale of differential scattering cross-section. The traditional method of using a powdered crystal is not appropriate for this since it makes determination of the relative scattering cross-section for the different isotopes of water unreliable. On the other hand, simply freezing liquid water in a container is also not suitable on its own since that method invariably leads to a high degree of preferred orientation in the sample, making a valid powder average impossible. The method adopted here to circumvent these problems was to freeze the water to 220 K, make the diffraction measurements, then thaw the sample. This cycle was repeated several times. After combining the data from all elements of the large detector array on SANDALS and from all freeze-thaw cycles, the result was effectively a powder average. The container in this case was a 1 mm thick slit in a 3 mm thick slab of zirconium–titanium alloy.

In all cases, the data analysis proceeded using the ATLAS data analysis suite [28], and the subsequent analysis of differential cross-section to HH, OH and OO partial structure factors used the polynomial method for subtracting the single atom scattering [29]. These data were then fit directly with a series of EPSR simulations under the conditions given in Table 1. Figs. 3–5 show fits to some of the diffraction data at 298, 573 and 673 K, whereas Figs. 6–9 show the derived OO, OH and HH radial distribution functions for all the states studied. Figs. 10–12 show the OO, OH and HH empirical potentials for the same states. Fig. 13 shows the fits to the ice data, whereas Fig. 14 shows the corresponding radial distribution functions. For this ice simulation, the starting point was an ensemble of molecules in the liquid state and there was only slight evidence that this simulation had started to form a crystalline structure, even after a lengthy simulation run, as discussed below.

Numerical tabulations of all these estimated radial distribution functions can be found at the website http://www.isis.rl.ac.uk/disordered.

4. Results

4.1. The reference potentials alone

Figs. 1 and 2 demonstrate that either of the chosen reference potentials produced a qualitative fit to the data, but disagreed in the detail. The SPC10 potential was used in an attempt to soften the repulsive core of the SPC/E potential. There is some evidence from the residual in the OO partial structure factor that the core is too hard in the Lennard-Jones term of this potential, making the first peak in the OO radial distribution unduly high and sharp. Changing the hardness of the core, meant that both the charges and the core diameter needed to be re-estimated to give the closest representation of the data. In the event however changing the hardness of the core potential from a 12th order power to 10th does not seem to affect this peak height unduly.

The configurational energy of the SPC10 potential was lower than that for the SPC/E parameters, but since configurational energies are not accurate in any of the present simulations this was not felt to be a serious deficiency. In general, the fits with SPC10 on its own are equivalent to those with the SPC/E parameters, although the SPC10 potential appears to capture the second peak in the OO radial distribution better than for SPC/E when the molecules are disordered. This is no doubt a consequence of the fact that the SPC/E potential was originally parameterised with localised atoms, and with slightly longer OH bonds than have been used here. It seems that once the atoms are delocalised, larger point charges are needed to compensate for the loss of intramolecular order.

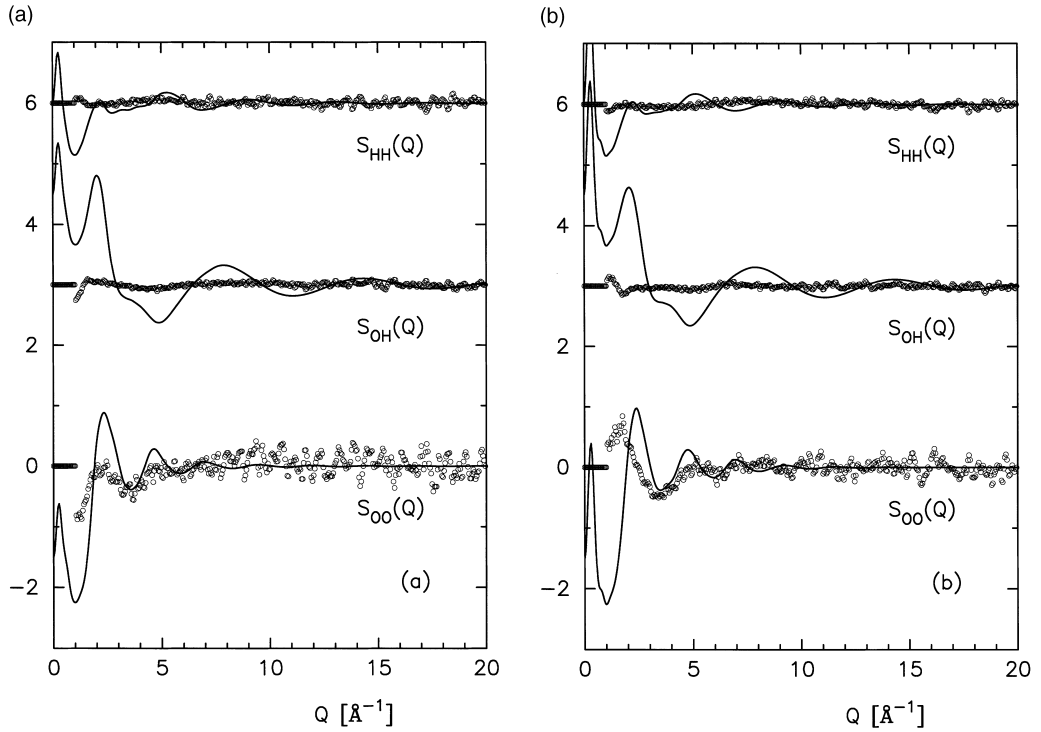

Fig. 4. EPSR fits to two datasets for water at 573 K, both at the same atomic number density of 0.072 atoms per Å^3 and pressure of 100 bar, which were measured at different times. These are given in Table 1 as 573a (a), and 573b (b). A considerable degree of similarity exists between the two datasets, albeit with some small differences.

Clearly, therefore, there is still scope for improvements to effective potential models such as the SPC/E model. Inclusion of a representation of intramolecular zero-point disorder will certainly be needed if a better fit to diffraction data is to be achieved.

4.2. Cold and ambient water

The radial distribution functions for cold water under pressure can be compared with those of ambient water. As has been discussed elsewhere [11,26], the primary effect of increasing water pressure is to modify the *second* water shell around a central water molecule, pulling it inwards, while changes to the first shell are relatively small. When this shell is pulled in it appears that it involves breaking the hydrogen-bonded network, allowing the H bonds that remain to become more linear. This is seen from the fact that the OO distance actually appears to *increase* slightly on increasing the pressure, whereas the OH intermolecular distance becomes smaller and better defined. If the hydrogen bonds were simply being bent by the application of pressure then the opposite to these tendencies would be expected.

Also of interest in the ambient water data is the new analysis of the old reactor neutron data compared to the same analysis of the more recent pulsed neutron data. The pulsed data were measured to much larger Q values than the reactor data. The residuals for the two datasets are different, in fact, the residuals for the reactor data are generally larger than for the time-of-flight data. Nonetheless, the resulting radial distribution functions from the two datasets are surprisingly close. This helps to establish the extent of systematic effects in these experiments. They are obviously non-trivial, particularly for the reactor experiment, but the computer simulation approach

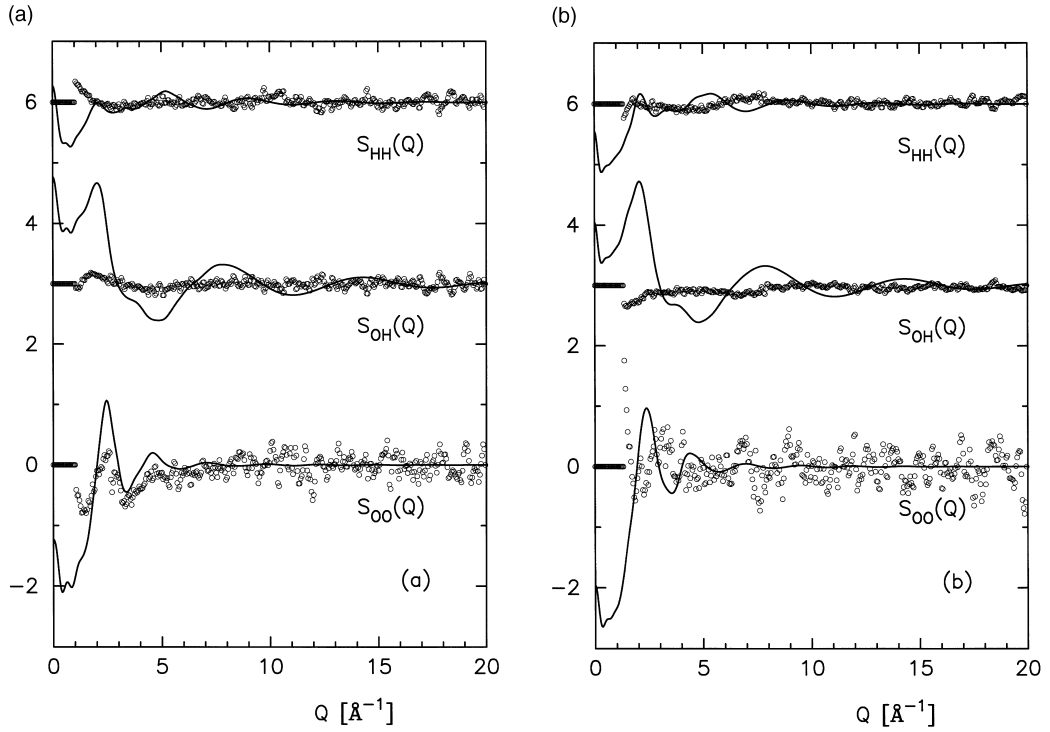

Fig. 5. EPSR fits to two datasets for water at 673 K, at atomic number densities of 0.066 atoms per Å^3 (673b (a)) and 0.073 atoms per Å^3 (673c (b)), which were measured at different times.

to estimate the radial distribution functions serves to prevent the worst artifacts in the data being transferred to the calculated functions.

4.3. Superheated and supercritical water

As the temperature is raised above the normal boiling point, the water network becomes progressively more disordered, so that by 573 K it has largely disappeared, and the hydrogen bond itself is considerably weakened. This can be seen from the disappearance of the 4.5 Å peak in the OO function, and the weakening of the first intermolecular peaks in the HH and OH functions. By 673 K the OH peak has weakened to the point of becoming a shoulder rather than a distinct peak, and in an earlier publication, we claimed this implied a complete breakdown of the hydrogen bond under these conditions [12]. Although the revised analysis of the supercritical data, both here and previously [18], gives more intensity to this peak than was originally indicated [12], it still shows up as a shoulder rather than the distinct peak that other simulations have indicated [30]. In fact, an angular definition for the hydrogen bond indicates that the level of hydrogen bonding between molecules has dropped to about 20% of its level in ambient water [31]. Other diffraction estimates indicate that a distinct OH peak may still be present [32] in supercritical water, but given the nature of possible truncation and systematic effects a final resolution of this matter remains elusive at present. Certainly, it is fair to claim that once the temperature is taken above the critical point, the hydrogen bonding in water becomes considerably depleted and this depletion is not fully reproduced by existing effective water potentials. Simulations using the Car–Parinello approach apparently give better agreement with the experiment than those with effective intermolecular potentials [33].

Two of the runs at 573 K, namely 573a and 573b, were measured at the same thermodynamic

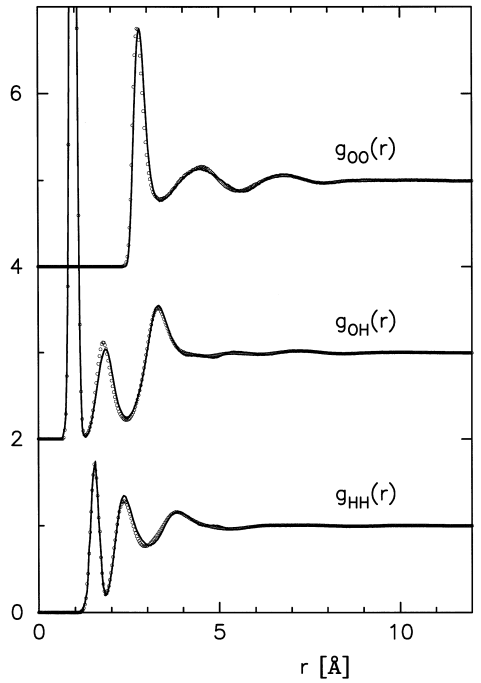

Fig. 6. Site–site radial distribution functions for water at 298 K, 1 bar, as derived from the two simulations used in Fig. 3. The simulations of the reactor data (Fig. 3(b)) are shown as dashed lines. It can be seen that although the systematic and truncation errors are different for the two datasets, the resulting radial distribution functions are closely similar.

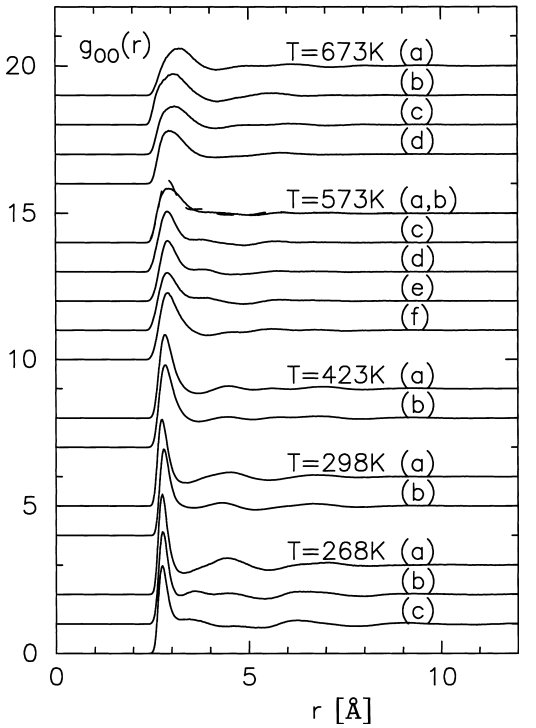

Fig. 7. Oxygen–oxygen, site–site radial distribution functions for water for the 17 state runs given in Table 1. Each curve is shifted by unity above its predecessor, except for run 573b which is shown as a dashed line on top of run 573a, because these two datasets were taken at different times but at the same thermodynamic state point. The comparison helps to establish the overall reliability of the reconstructions.

state point but separated in time by more than one year. Small differences between the refinements of these datasets are visible (Fig. 5), and these translate to differences in the estimated radial distribution functions (Figs. 7–9). These differences are an indication of the likely uncertainties in the extracted radial distribution functions. For superheated water systematic differences from one run to the next appear to have an effect at the 10% level in the estimated radial distribution functions at short distances, and these differences almost certainly account for the reported discrepancies between different datasets. It will be seen that the discrepancies occur not only on peak amplitudes, but also on peak positions. The problem of transferred systematic error is particularly acute for superheated water, because it is possible to have only a relatively small amount of sample in the beam (about 20% of that for the ambient data), while at the same time the inelasticity distortions are enhanced by the increased temperature.

In spite of these reservations, some general trends are seen in the radial distribution functions of Figs. 7–9. In particular, a general movement of the OO peak to larger distances is seen as the temperature is raised and the density lowered. The same peak also becomes broader and less well defined. At the same time, the first OH intermolecular peak broadens out and also moves to larger distances on average, as does to a lesser extent the first intermolecular HH peak. However, for the second peak in the OH and HH functions there appears to be little movement with thermodynamic state point.

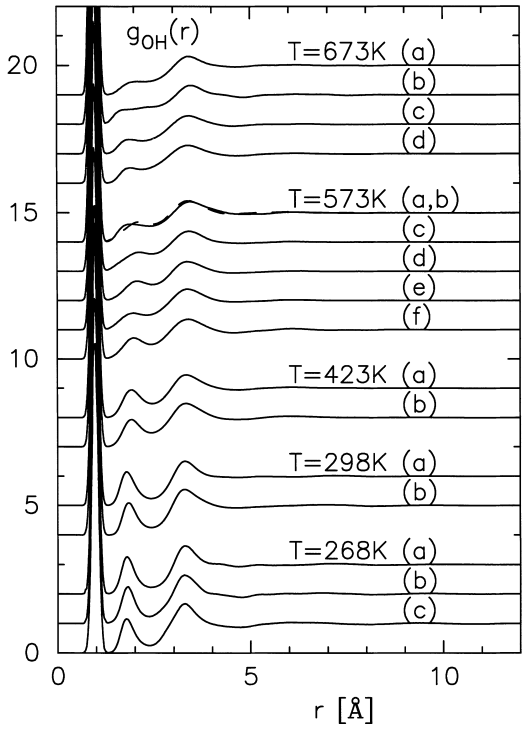

Fig. 8. Same as in Fig. 7, but for the OH radial distribution functions.

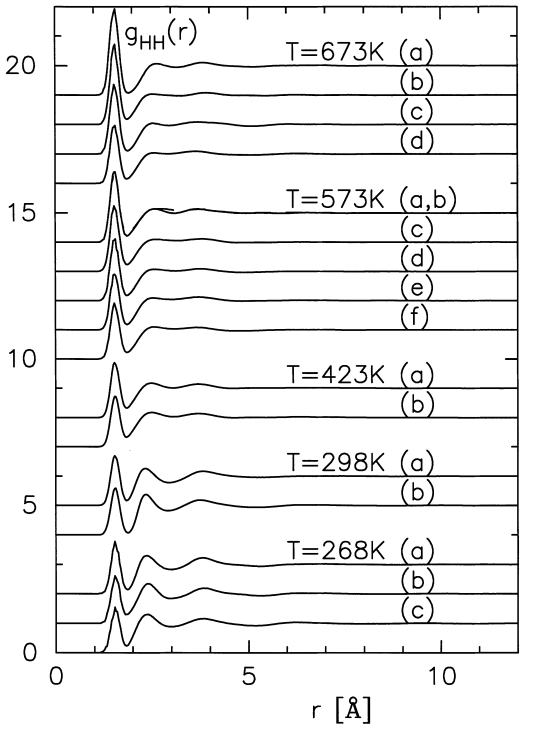

Fig. 9. Same as in Fig. 7, but for the HH radial distribution functions.

4.4. Empirical potentials, 268–673 K

Figs. 10–12 show the empirical potentials obtained from the structure refinements of water. These are the overall perturbations that have to be added to the SPC/E parameterisation of the reference potential to reproduce the radial distribution functions shown in Figs. 7–9. Considerable variation between the different potentials is apparent, particularly in the OO and OH potentials. In particular, it may be discerned that the potentials derived from data measured in the same batch of experiments tend to have similar features which are often significantly different from those derived from another batch of experiments. The runs that can be grouped into batches of data taken within a few days of each other are [268a,268b,268c]; [423a,423b,573f]; [573b,573c,573d,573e]; [573a, 673b]; and [673a,673c,673d]. By comparison, the separation between the batches of runs is often several months or even a few years in some cases. It is clear therefore that considerable uncertainty remains about the true nature of the empirical potential for water. The OO empirical potential is perhaps the most uncertain of the three. This no doubt reflects the general difficulty in obtaining a reliable OO partial structure factor for water, particularly under conditions of high pressure and temperature. It should be borne in mind however that the amplitudes of these empirical potentials are typically an order of magnitude or more smaller than the corresponding Coulomb potentials, so they do represent relatively small perturbations to the overall intermolecular potential. Perhaps, it is not overly surprising therefore that they have a high degree of uncertainty.

It is possible however to make a few comments about some general trends that can be discerned in these figures. At temperatures up to 423 K, the OH empirical potential is generally attractive (positive gradient) at the normal hydrogen bond distance around 1.9 Å. At 673 K, it tends to be repulsive

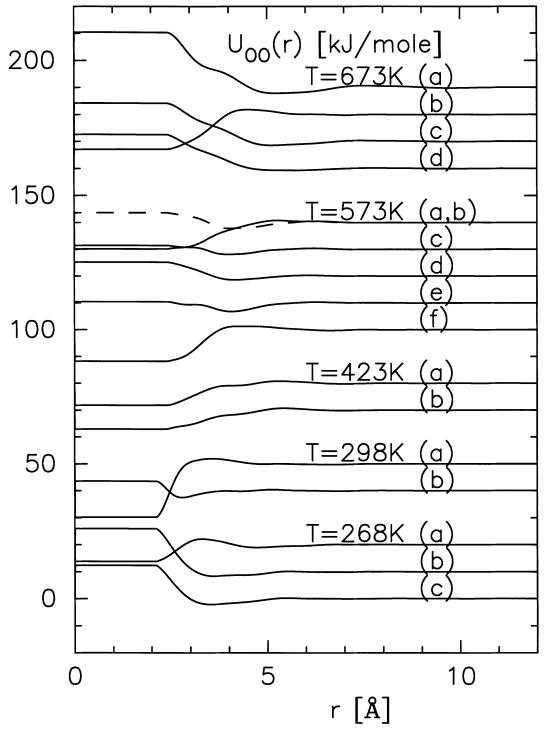

Fig. 10. Oxygen–oxygen empirical potentials derived from the EPSR simulation of the 17 datasets of Table 1 for water, using the SPC/E parameterisation of the reference potential. The potentials are shown in five bands corresponding to the 5 temperature bands of Table 1, namely 268 K (three pressures), 298 K (two pressures), 423 K (two pressures), 573 K (five pressures, six experiments), and 673 K (four pressures). For clarity, each band is shifted upwards by 20 kJ mol^{-1} from the preceding band. Within each band, each pressure is separated from its neighbour by 10 kJ mol^{-1} with the highest pressure at the *bottom* of each band. The curve labelling corresponds to that used in the table. As with the radial distribution functions, the potential for run 573b is shown as a dashed line overlapping that for run 573a because these two runs corresponded to the same thermodynamic state point.

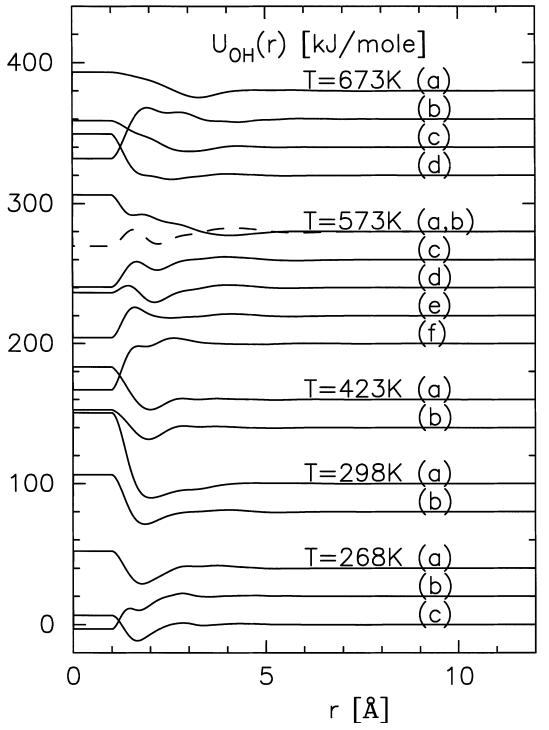

Fig. 11. Same as in Fig. 10, but for the OH empirical potentials.

(negative gradient) at this distance range, while at 573 K it's slope is not well defined. Although there is greater variability, the OO empirical potential shows a similar trend at the near neighbour distance, 2.8 Å. Meanwhile the HH potential shows no obvious variation, being generally slightly repulsive at the near-neighbour intermolecular distance. There is therefore some evidence here that polarisation effects are important in the water potential. At lower temperatures and higher densities, the OH attraction tends to be stronger than that given by the charge model, resulting in a slightly attractive empirical potential. At higher temperatures and lower densities, where the degree of polarisation is reduced, the OH potential becomes mildly repulsive compared to the fixed charge model. It will be interesting to see whether these general trends can help to establish a useful model for the effects of polarisation in the intermolecular water potential.

In addition, the fact that the OO potential tends be attractive at short distances and at lower temperatures and densities suggests that the assumed repulsive core potential is too hard under these conditions, and a softer core is required. Alternatively, this could equally be regarded as another indication of polarisation effects: a larger charge on the hydrogen atoms will lead to a stronger hydrogen-bond than for the reference potential on its own, pulling the molecules slightly closer together.

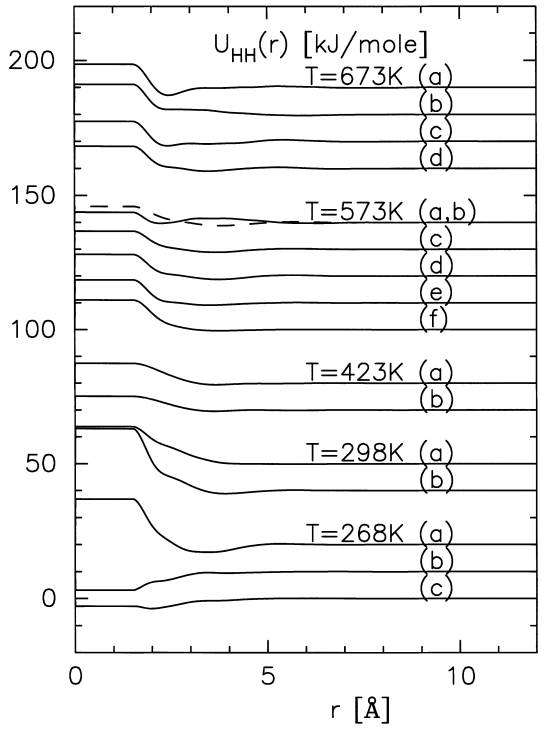

Fig. 12. Same as in Fig. 10, but for the HH empirical potentials.

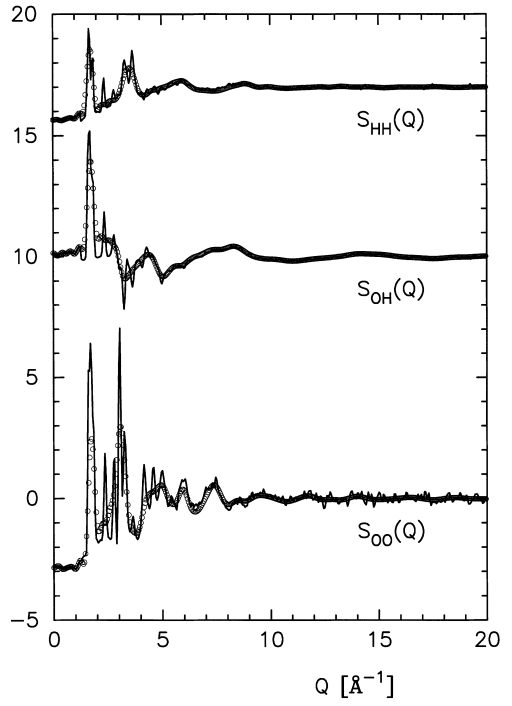

Fig. 13. EPSR fits to the OO, OH and HH partial structure factors of ice Ih at 220 K, 1 bar. The lines show the measured data, while the circles are the EPSR fits.

4.5. Fits to the ice data

The fits to the ice data are shown in Fig. 13, with the corresponding radial distribution functions in Fig. 14. Obviously, the crystalline nature of ice means that a complete representation of the diffraction data cannot be achieved with the EPSR method in its present form. There is some evidence that the simulated ensemble of water molecules has started to crystallise, as seen by the sharpness of the peaks in Q space. But clearly the true long range order of ice is not correctly represented here. This is a subject for a more detailed discussion elsewhere, but it is important to emphasise that in fact the short range structure out to about $r = 5$ Å is accurately represented by the EPSR radial distribution functions. Fourier transform of the residuals shown in Fig. 14 reveals little missing structure in any of the three site–site radial distribution functions out to this distance range. The fact that the method does not reproduce the sharp Bragg peaks is a consequence of the smallness of the box used. A box of dimension at least five times bigger than the present one would be needed if a more accurate representation of the Bragg peaks were to be achieved. At this point, such a large simulation has not been attempted. A key question of course would be to see whether it would crystallise into the correct structure for ice Ih.

What is clear from this simulation is that significant short range *disorder* is prevalent in ice at 220 K: this can be seen from the significant width of the first intermolecular peaks in both the HH (2.2 Å) and OH (1.7 Å) peaks. Also, after the first peak in the OO distribution there is non-zero intensity near 3.4 Å indicating some residual interstitial atoms in the lattice. (The density in this region would go to zero if the lattice were perfect.) The use of partial structure factors in this case demonstrates that direct crystallographic methods may miss some of the local detail in the lattice.

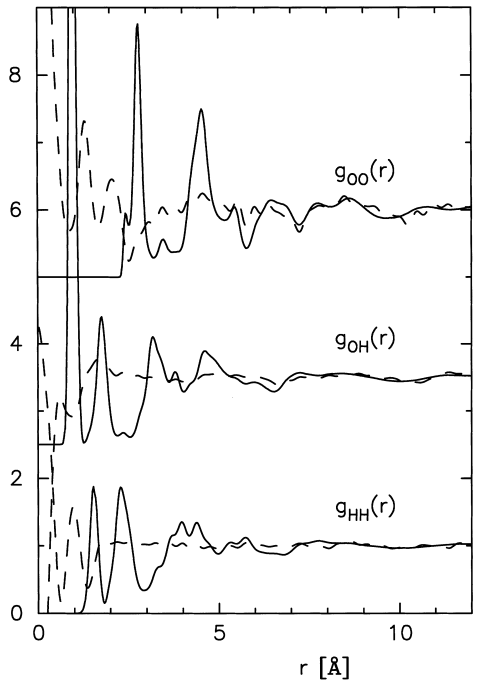

Fig. 14. Site–site radial distribution functions (—) from the EPSR simulations of Fig. 13. The dashed lines show the Fourier transform of the difference between diffraction data and EPSR fit. They indicate that most of the intermolecular structure in the region 2–5 Å has been captured by the EPSR simulation, although the longer range structural oscillations are too weak compared to what would be required to reproduce the observed Bragg peaks.

5. Discussion

According to the results presented here, our earlier calculation of the OH and OO radial distribution functions in ambient water [1] appeared to overestimate the sharpness and height of the first intermolecular peak in each of these functions. This is because a Gaussian function was used to represent each of these peaks, the height and width of which was adjusted to give the best fit to the data, which extended to a maximum Q of about 10 Å^{-1}. The more recent time-of-flight diffraction data extend to 40 Å^{-1} and were fit to 20 Å^{-1} in the present simulations. The smallness of the Q range of the reactor data appears to introduce a significant limitation on the accuracy to which peak heights can be estimated. However, the discrepancies between the present estimates and the earlier published results does give an indication of the uncertainty in the height and width of these peaks. It emphasises again the difficulty of comparing a computer simulation from a finite box of molecules in real space with experimental diffraction data in reciprocal space. The two activities do measure formally distinct quantities, and any statements to the effect that one simulation fits the data better or worse than another simulation can be really only be sustained if the comparison is done in experimental reciprocal space.

The present simulations demonstrate that it is possible to make this comparison for liquid water provided the simulation box is large enough. The method fails in the event the correlations becoming longer ranged than the size of the box used in the simulation. This was seen here in the case of ice, and would probably occur for amorphous solid water if partial structure factor data were available. However, even when long range order exists, the short range order in the material can still apparently be represented in these cases.

One remaining question to be discussed concerns the likelihood of improving the quality of the data to resolve the remaining discrepancies. This will require diffraction data with a statistical precision at least 3–6 times better than is currently available at high Q values, requiring a 10- to 30-fold increase in source intensity. In principle, X-rays should be able to obtain better statistics than neutrons. However, the realities of needing to estimate or measure the Compton scattering, and to know the electron form factors to very good accuracy, has so far precluded any serious attempt to improve the quality of the data at large Q. In any case, X-rays will measure the OO structure factor to good accuracy, but yield little information on the OH and HH functions. A new neutron source and associated instrumentation with the necessary flux advantage will not be available for 5–10 years. In this situation, the present estimates, using the computer simulation approach to reduce the contribution of artifacts in the data, are probably the best estimates of the radial distribution functions of water available at the present time.

The EPSR method also appears to be able discern some general trends in the intermolecular

water potential with temperature and density. On the basis of the evidence in Figs. 10–12, it appears that polarisation effects on the intermolecular potential may be significant for determining the local structure at short distances. Simple point charge models of water are obviously good over a range of state conditions, but it is likely that an accurate potential will have to include a many-body dependence, such as a polarisability term.

6. Conclusion

The method of EPSR has been used here to estimate the site–site radial distribution functions for water for a series of thermodynamic state points ranging from ice at 220 K to supercritical water at 673 K, and including pressures up to 400 MPa. The inputs to this structure refinement are the measured HH, OH and OO partial structure factors as obtained in neutron diffraction experiments using hydrogen/deuterium isotope substitution. Comparison of structure refinements on different datasets measured at different times but under the same thermodynamic states gives an indication of the likely uncertainties in the radial distribution functions obtained from diffraction experiments. Using this method of analysis, which fits all three partial structure factors simultaneously, the estimated functions appear more robust than earlier estimates. Likely improvements in the data can be considered, but qualitative changes to the intensity of current neutron and X-ray sources will be needed before the remaining controversies can be resolved.

References

[1] A.K. Soper, M.G. Phillips, Chem. Phys. 107 (1986) 47.
[2] C. Andreani, M. Nardone, F.P. Ricci, A.K. Soper, Phys. Rev. A 46 (1992) 4709.
[3] C. Andreani, F. Menzinger, M.A. Ricci, A.K. Soper, J. Dreyer, Phys. Rev. B 49 (1994) 3811.
[4] C. Andreani, M.A. Ricci, A.K. Soper, J. Chem. Phys. 107 (1997) 214.
[5] G. Santoli, F. Bruni, F.P. Ricci, M.A. Ricci, A.K. Soper, Mol. Phys. 97 (1999) 777.
[6] M.A. Ricci, M. Nardone, F.P. Ricci, C. Andreani, A.K. Soper, J. Chem. Phys. 102 (1995) 7650.
[7] A.K. Soper, R.N. Silver, Phys. Rev. Lett. 49 (1982) 471.
[8] A.K. Soper, Physica 136B (1986) 322.
[9] R.A. Kuharski, P.J. Rossky, J. Chem. Phys. 82 (1985) 5164.
[10] J.H. Root, P.A. Egelstaff, A. Hime, Chem. Phys. 109 (1986) 437.
[11] A.V. Okhulkov, Yu.N. Damianets, Yu.E. Gorbaty, J. Chem. Phys. 100 (1994) 1578.
[12] P. Postorino, R.H. Tromp, M.A. Ricci, A.K. Soper, G.W. Neilson, Nature 366 (1993) 668.
[13] A. Chialvo, P.T. Cummings, J. Chem. Phys. 101 (1994) 4466.
[14] G. Löffler, H. Schreiber, O. Steinhauser, Ber. Bunsen-Ges. Phys. Chem. 98 (1994) 1575.
[15] L. Pusztai, Phys. Rev. B 60 (1999) 11851.
[16] M.-C. Bellisent-Funel, Hydrogen Bonded Liquids, in: J.C. Dore, J. Teixeira (Eds.), NATO ASI Ser C 329 (1991) 117.
[17] M.-C. Bellisent-Funel, R. Sridi-Dorrez, L. Bosio, J. Chem. Phys. 104 (1996) 1.
[18] A.K. Soper, F. Bruni, M.A. Ricci, J. Chem. Phys. 106 (1997) 247.
[19] P. Jedlovsky, I. Bako, G. Palinkas, T. Radnai, A.K. Soper, J. Chem. Phys. 105 (1996) 245.
[20] A.K. Soper, Chem. Phys. 202 (1996) 295.
[21] H.J.C. Berendsen, J.R. Grigera, T.P. Straatsma, J. Phys. Chem. 91 (1987) 6269.
[22] A.K. Soper, C. Andreani, M. Nardone, Phys. Rev. E 47 (1993) 2598.
[23] I. Nezbeda, J. Kolafa, Mol. Phys. 97 (1999) 1105.
[24] M.P. Allen, D.J. Tildesley, Computer Simulation of Liquids, Oxford University Press, Oxford, 1989.
[25] R. Leberman, A.K. Soper, Nature 378 (1995) 364.
[26] A.K. Soper, M.A. Ricci, Phys. Rev. Lett. 84 (2000) 2881.
[27] P. Postorino, M.A. Ricci, A.K. Soper, J. Chem. Phys. 101 (1994) 4123.
[28] ATLAS-Analysis of Time-of-Flight Diffraction Data from Liquid and Amorphous Samples, in: A.K. Soper, W.S. Howells, A.C. Hannon (Eds.), Rutherford Appleton Laboratory Report RAL-89-046, 1989.
[29] A.K. Soper, A. Luzar, J. Chem. Phys. 97 (1992) 1320.
[30] A.G. Kalinichev, J.D. Bass, J. Phys. Chem. 101 (1997) 9720 and references therein.
[31] A.K. Soper, Farad. Disc. 103 (1996) 41.
[32] T. Tassaing, M.-C. Bellisent-Funel, B. Guillot, Y. Guissani, Europhys. Lett. 42 (1998) 265.
[33] E.S. Fois, M. Sprik, M. Parinello, Chem. Phys. Lett. 223 (1994) 411.